

Synthesis, NMR and Vibrational Spectroscopic Characterization, and Computational Study of the *cis*- $\text{IO}_2\text{F}_3^{2-}$ Anion

Johnathan P. Mack,[†] Jerry A. Boatz,[‡] and Michael Gerken^{*,†}

Department of Chemistry and Biochemistry, The University of Lethbridge, Lethbridge, Alberta T1K 3M4, Canada, and the Air Force Research Laboratory, Edwards Air Force Base, California 93524

Received November 16, 2007

The $\text{N}(\text{CH}_3)_4^+$ salt of the *cis*- $\text{IO}_2\text{F}_3^{2-}$ anion was synthesized from $[\text{N}(\text{CH}_3)_4][\text{IO}_2\text{F}_2]$ and excess $[\text{N}(\text{CH}_3)_4][\text{F}]$ in CH_3CN solvent. The $[\text{N}(\text{CH}_3)_4]_2[\text{IO}_2\text{F}_3]$ salt was characterized by Raman, infrared, and ^{19}F solid-state MAS NMR spectroscopy. Geometry optimization and calculation of the vibrational frequencies at the DFT level of theory corroborated the experimental finding that the $\text{IO}_2\text{F}_3^{2-}$ anion exists as a single isomer with a *cis*-dioxo and *mer*-trifluoro arrangement. The fluorine atom in $\text{IO}_2\text{F}_3^{2-}$ that is trans to one of the oxygen atoms is weakly bound with a calculated bond length of 228.1 pm. The $\text{IO}_2\text{F}_3^{2-}$ anion is only the second example of an AEO_2F_3 species after XeO_2F_3^- .

Introduction

Iodine fluorides and oxide fluorides have been extensively investigated to study the relative repulsive effects of single-bonds to fluorines, double-bonds to oxygens, and lone pairs, in order to verify geometry predictions using the VSEPR model.¹ Three octahedral iodine(VII) fluorides and oxide fluorides have been prepared, IF_6^+ ,² IOF_5 ,³ and IO_2F_4^- ,⁴ being AX_6 , AYX_5 , and AY_2X_4 molecules, respectively. Interestingly, the IO_2F_4^- anion was found to exist as a mixture of the *cis*- and *trans*-isomer, with the *cis*-isomer being an exception to the VSEPR rules. Prior to this study only two pseudo-octahedral iodine(V) fluorides and oxide fluorides were known, i.e., IF_5 ⁵ and IOF_4^- ,⁶ being AEX_5 and AEYX_4 VSEPR molecules, respectively. In addition, a few other pseudo-octahedral iodine(V) fluoride compounds have been reported, such as the organo-iodine(V) fluorides CF_3

IF_4^7 and $\text{C}_6\text{F}_5\text{IF}_4$.⁸ Iodine(V) oxide fluorides make possible the comparison between the repulsive effects of lone pairs and bonding pairs. The repulsion caused by a lone pair can be very similar to that of a double bond.

The availability of anhydrous $[\text{N}(\text{CH}_3)_4][\text{F}]$ ⁹ has resulted in the preparation of a number of iodine fluoride and oxide fluoride dianions, such as the $\text{IO}_2\text{F}_5^{2-}$,¹⁰ IOF_5^{2-} ,¹¹ and IF_5^{2-} ¹² anions. The lack of any report of an iodine AEO_2X_3 species sparked interest in the synthesis of the $\text{IO}_2\text{F}_3^{2-}$ anion and investigation of its geometry and possible isomerism. Prior to this study, XeO_2F_3^- was the only AEO_2F_3 species that has been synthesized,^{13,14} which was shown to have a *cis*-dioxo arrangement based on the vibrational spectroscopy of its Cs^+ salt.¹⁴

Results and Discussion

Synthesis of $[\text{N}(\text{CH}_3)_4]_2[\text{IO}_2\text{F}_3]$. The $\text{N}(\text{CH}_3)_4^+$ salt of the IO_2F_2^- anion reacts with a 4-fold molar excess of

* To whom correspondence should be addressed. Tel.: (403) 329-2173. Fax: (403) 329-2057. E-mail: michael.gerken@uleth.ca.

[†] University of Lethbridge.

[‡] Air Force Research Laboratory.

- (1) (a) Gillespie, R. J.; Hargittai, I. *The VSEPR Model of Molecular Geometry*; Allyn and Bacon, A Division of Simon & Schuster: Needham Heights, MA, 1991. (b) Gillespie, R. J.; Popelier, P. L. A. *Chemical Bonding and Molecular Geometry: From Lewis to Electron Densities*; Oxford University Press: Oxford, U.K., 2001.
- (2) Lehmann, J. F.; Schrobilgen, G. J.; Christe, K. O.; Kornath, A.; Suontamo, R. J. *Inorg. Chem.* **2004**, *43*, 6905–6921.
- (3) Christe, K. O.; Curtis, E. C.; Dixon, D. A. *J. Am. Chem. Soc.* **1993**, *115*, 9655–9658.
- (4) Christe, K. O.; Wilson, D. W.; Schack, C. J. *Inorg. Chem.* **1981**, *20*, 2104–2114.
- (5) Balıkcı, B.; Brier, P. N. *J. Mol. Spectrosc.* **1981**, *89*, 254–260.
- (6) Ryan, R. R.; Asprey, L. B. *Acta Crystallogr. Sect. B* **1972**, *28*, 979.

(7) Minkwitz, R.; Bröchler, R.; Preut, H. Z. *Anorg. Allg. Chem.* **1995**, *621*, 1247–1250.

(8) Frohn, H. J.; Görg, S.; Henkel, G.; Läge, M. Z. *Anorg. Allg. Chem.* **1995**, *621*, 1251–1256.

(9) Christe, K. O.; Wilson, W. W.; Wilson, R. D.; Bau, R.; Feng, J.-A. *J. Am. Chem. Soc.* **1990**, *112*, 7619–7625.

(10) Boatz, J. A.; Christe, K. O.; Dixon, D. A.; Fir, B. A.; Gerken, M.; Gnann, R. Z.; Mercier, H. P. A.; Schrobilgen, G. J. *Inorg. Chem.* **2003**, *42*, 5282–5292.

(11) Christe, K. O.; Wilson, W. W.; Dixon, D. A.; Boatz, J. A. *J. Am. Chem. Soc.* **1999**, *121*, 3382–3385.

(12) Christe, K. O.; Wilson, W. W.; Drake, G. W.; Dixon, D. A.; Boatz, J. A.; Gnann, R. Z. *J. Am. Chem. Soc.* **1998**, *120*, 4711–4716.

(13) Gillespie, R. J.; Schrobilgen, G. J. *Chem. Commun.* **1977**, 595–597.

(14) Christe, K. O.; Wilson, W. W. *Inorg. Chem.* **1988**, *27*, 3763–3768.

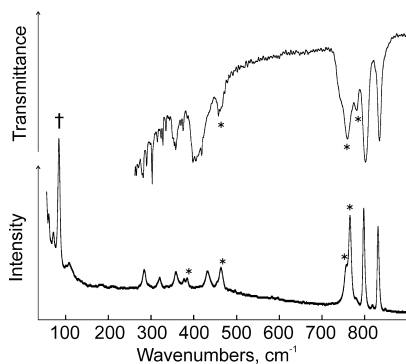
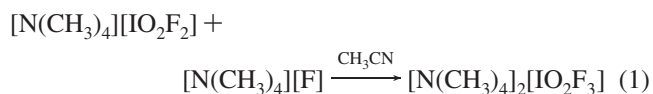
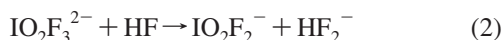


Figure 1. Vibrational spectra of $[\text{N}(\text{CH}_3)_4]_2[\text{IO}_2\text{F}_3]$ containing about 75 mol % $[\text{N}(\text{CH}_3)_4][\text{F}]$: Raman spectrum (lower trace) recorded at $-100\text{ }^\circ\text{C}$ using 1064-nm excitation and the infrared spectrum (upper trace) recorded at room temperature in an AgCl pellet. Asterisks (*) and dagger (†) denote $\text{N}(\text{CH}_3)_4^+$ bands and a laser line, respectively.

$[\text{N}(\text{CH}_3)_4][\text{F}]$ in CH_3CN at $-32\text{ }^\circ\text{C}$ for ca. 100 h yielding the colorless $[\text{N}(\text{CH}_3)_4]_2[\text{IO}_2\text{F}_3]$ salt in admixture with $[\text{N}(\text{CH}_3)_4][\text{F}]$ according to eq 1.



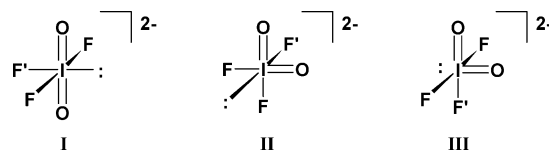
The use of stoichiometric amounts of $[\text{N}(\text{CH}_3)_4][\text{F}]$ resulted in initial formation of small amounts of $[\text{N}(\text{CH}_3)_4]_2[\text{IO}_2\text{F}_3]$ and its subsequent solvent attack to form $[\text{N}(\text{CH}_3)_4]_2[\text{HF}_2][\text{IO}_2\text{F}_2]$, which was identified by vibrational spectroscopy.¹⁵ The solvent attack of anhydrous $[\text{N}(\text{CH}_3)_4][\text{F}]$ in CH_3CN at temperatures higher than $-20\text{ }^\circ\text{C}$ is well-documented,⁹ however, the formation of bifluoride at temperatures below $-30\text{ }^\circ\text{C}$ is unprecedented. Extraction of $[\text{N}(\text{CH}_3)_4][\text{F}]$ from the $[\text{N}(\text{CH}_3)_4]_2[\text{IO}_2\text{F}_3]$ - $[\text{N}(\text{CH}_3)_4][\text{F}]$ mixture at low temperature also led to formation of $[\text{N}(\text{CH}_3)_4]_2[\text{HF}_2][\text{IO}_2\text{F}_2]$. In the absence of a sufficient excess of $[\text{N}(\text{CH}_3)_4][\text{F}]$, the $\text{IO}_2\text{F}_3^{2-}$ anion apparently promotes proton abstraction from CH_3CN , even at $-30\text{ }^\circ\text{C}$. The generated HF acts as a better fluoride-ion acceptor than the IO_2F_2^- anion (eq 2), preventing the isolation of $\text{IO}_2\text{F}_3^{2-}$ salts under stoichiometric conditions.



Vibrational Spectroscopy. The Raman and infrared spectra of $[\text{N}(\text{CH}_3)_4]_2[\text{IO}_2\text{F}_3]$ containing about 3-fold molar excess of $[\text{N}(\text{CH}_3)_4][\text{F}]$ are shown in Figure 1. The observed vibrational frequencies for $\text{IO}_2\text{F}_3^{2-}$ and their assignments based on the theoretical calculations are summarized in Table 1. In addition to the vibrational bands attributable to unreacted $[\text{N}(\text{CH}_3)_4][\text{F}]$ and to the $\text{N}(\text{CH}_3)_4^+$ cation of the $[\text{N}(\text{CH}_3)_4]_2[\text{IO}_2\text{F}_3]$ salt, nine and four anion bands were observed in the Raman and infrared spectra, respectively.

Three structures are conceivable for the $\text{IO}_2\text{F}_3^{2-}$ anion; a *trans*- $\text{IO}_2\text{F}_3^{2-}$ (I) isomer of C_{2v} symmetry and two *cis*- $\text{IO}_2\text{F}_3^{2-}$ isomers (II) and (III), both having C_s symmetry.

The lone pair in a *trans*-dioxo arrangement would result in a slight deviation from linearity of the O–I–O moiety.



Nevertheless, close to mutual exclusive behavior of the Raman and infrared bands is expected, as is a large separation of the two I–O stretching modes due to maximum coupling of these modes. Strict mutual exclusion has been observed in vibrational spectra of *trans*- $\text{IO}_2\text{F}_5^{2-}$ ¹⁰ and *trans*- $\text{IO}_2\text{F}_4^{-4}$ anions, in which both anions contain linear IO_2 moieties. In the Raman and infrared spectra of $[\text{N}(\text{CH}_3)_4]_2[\text{IO}_2\text{F}_3]$, two intense I–O stretching bands were observed at 832 (Raman)/834 (infrared) and 798 (Raman)/802 (infrared) cm^{-1} , consistent with a *cis*-dioxo arrangement in the $\text{IO}_2\text{F}_3^{2-}$ anion. Furthermore, it was found by computational means that the *trans*- $\text{IO}_2\text{F}_3^{2-}$ (I) isomer is not a local minimum on the ground-state potential energy surface (see Computational Results). The presence of a mixture of isomers was excluded based on the number of observed I–O stretching bands and on the solid-state NMR spectroscopic results (see Solid-State NMR Spectroscopy).

A total of 12 vibrational modes are expected for isomers II and III of the *cis*- $\text{IO}_2\text{F}_3^{2-}$ anion, which span the irreducible representations $\Gamma = 7A' + 5A''$ and $\Gamma = 8A' + 4A''$, respectively, in the C_s point group, with all modes being Raman and infrared active. Isomer II is predicted to be less stable than isomer III by 46 kJ/mol. Furthermore, the predicted infrared and Raman vibrational spectra of (III) are in better agreement with experiment than those of (II), which suggests that the former is the experimentally observed isomer. Examination of the potential energy distribution (PED, not shown) of isomer III reveals that the two I–O stretching bands at 832 and 798 cm^{-1} are only weakly coupled with each other and are characteristic of the stretching of the I–O bonds *cis*, $\nu(\text{IO}_{\text{cis}})$, and *trans*, $\nu(\text{IO}_{\text{trans}})$, to the I–F' bond, respectively. The lower frequency of $\nu(\text{I}-\text{O}_{\text{trans}})$ compared to that of $\nu(\text{I}-\text{O}_{\text{cis}})$ is a consequence of the *trans*-effect of the I–F' bond, rendering the I– O_{trans} bond more ionic than I– O_{cis} . Three I–F stretching bands were observed at 432, 405, and 358 cm^{-1} . The latter band primarily involves the stretching of the weak I–F' bond, combined in an out-of-phase fashion with the symmetric IF_2 stretch. Compared with the I–O stretching (849 and 818 cm^{-1}) and I–F stretching (468 and 445 cm^{-1}) frequencies of the IO_2F_2^- anion, the lower stretching frequencies for the *cis*- $\text{IO}_2\text{F}_3^{2-}$ anion are consistent with an increase of ionic character of the bonds in the dianion. As observed for iodine *trans*-dioxo species, the increased bond polarization upon increasing the ionic charge is more pronounced for the I–F bonds than for the I–O bonds.¹⁰ This is a direct consequence of the higher electronegativity of fluorine versus oxygen. The comparison of the stretching frequencies of *cis*- $\text{IO}_2\text{F}_3^{2-}$ with *cis*- IO_2F_4^- , which are related by formal replacement of a fluorine atom by a lone pair, reveals an even larger increase in polarization of the I–O and I–F bonds when decreasing the oxidation state on iodine from +VII to +V. Such an

(15) Gerken, M.; Mack, J. P.; Schrobilgen, G. J.; Suontamo, R. J. *J. Fluorine Chem.* **2004**, *125*, 1663–1670.

Table 1. Observed and Calculated Vibrational Frequencies of Isomers II and III of *cis*-IO₂F₃²⁻ and Their Assignment in Point Group C_s

[N(CH ₃) ₄][IO ₂ F ₃]		Frequencies, ^a cm ⁻¹				
		IO ₂ F ₃ ²⁻ , isomer II		IO ₂ F ₃ ²⁻ , isomer III		
Raman ^b	infrared ^c	calcd ^d	assignments	calcd ^d	assignments	
832 [86]	834 s	720 (214) [14]	$\nu_8(A'')$, $\nu_{as}(IO)$	764 (120) [19]	$\nu_1(A')$, ν (IO _{cis})	
798 [100]	802 s	718 (122) [36]	$\nu_1(A')$, $\nu_a(IO)$	722 (184) [31]	$\nu_2(A')$, ν (IO _{trans})	
432 [18]		446 (155) [13]	$\nu_2(A')$, $\nu_a(IF')$	382 (48) [15]	$\nu_3(A')$, $\nu_s(IF_3)$	
-	405 s	366 (127) [4]	$\nu_3(A')$, $\nu_a(IF)$	417 (318) [0]	$\nu_9(A'')$, $\nu_{as}(IF_2)$	
358 [11]	358 m	336 (109) [6]	$\nu_9(A'')$, $\nu_{as}(IF)$	328 (106) [5]	$\nu_4(A')$, $\nu_{as}(IF_3)$	
320 [9]	-	316 (12) [5]	$\nu_4(A')$, $\delta_{scissoring}(IO_2)$	301 (17) [5]	$\nu_5(A')$, $\delta_{scissoring}(IO_2)$	
284 [18]	-	248 (22) [4]	$\nu_5(A')$, $\delta_s(OIF')$	245 (0.1) [3]	$\nu_{10}(A'')$, $\delta_{as}(IF_2)$	
210 [2]	-	241 (0.2) [2]	$\nu_{10}(A'')$, $\delta_{as}(OIF')$	215 (0) [4]	$\nu_{11}(A'')$, $\delta_{as}(IF_2)$	
180 [3]	-	176 (17) [2]	$\nu_6(A')$, $\delta_s(FIF')$	186 (33) [1]	$\nu_6(A')$, $\delta_{scissoring}(IF_2)$	
-	-	174 (1.1) [1]	$\nu_{11}(A'')$, $\delta_{scissoring}(OIF)$	148 (1) [0.3]	$\nu_7(A')$, $\delta_{scissoring}(IF_2)$	
-	-	140 (2.8) [1]	$\nu_7(A')$, $\delta_{scissoring}(FIF)$	114 (0.2) [0]	$\nu_8(A')$, $\delta_{puckering}(IOF_3 \text{ plane})$	
108 [10]	-	108 (0.57) [0.3]	$\nu_{12}(A'')$, $\delta_{puckering}(IO_2F_2 \text{ plane})$	94 (1) [1]	$\nu_{12}(A'')$, δ (F ₂ IF')	

^a Abbreviations denote shoulder (sh), very strong (vs), strong (s), medium (m), weak (w), and very weak (vw). ^b The N(CH₃)₄⁺ cation modes were observed in the Raman spectrum (-100 °C) at 377 (9), 385 (11), $\nu_8(E)$; 464 (22), $\nu_{19}(F_2)$; 758sh, 766 (91) (N(CH₃)₄F), $\nu_3(A_1)$; 955 (25), 966 (66) (N(CH₃)₄F), 972sh, $\nu_{18}(F_2)$; 1196 (5), 1208 (22), $\nu_7(E)$; 1296 (4), 1310 (5), $\nu_{17}(F_2)$; 1409(8), 1420 (11), $\nu_{16}(F_2)$; 1465(34), 1477(66) (N(CH₃)₄F), $\nu_2(A_1)$; 1487 (32), 1491sh, 1514 (14), $\nu_6(E)$; 2619(3), 2728(4), 2816 (51), 2826sh, 2841 (39), 2885(70), 2906sh, 2920sh, 2973 (84), 3009 (103), 3029 (114) cm⁻¹, ν_{CH_3} and binary bands (see refs 9 and 16). ^c The N(CH₃)₄⁺ cation modes were observed in the infrared spectrum at 463w, $\nu_{19}(F_2)$; 741sh, 760m, 783w, $\nu_3(A_1)$; 926 w, 2 ν_{19} ; 949vs, 957vs, 967s (N(CH₃)₄F), $\nu_{18}(F_2)$; 1257 s, $\nu_{17}(F_2)$; 1406 m, $\nu_{16}(F_2)$; 1488vs, 1503vs, 1522 vs, $\nu_{15}(F_2)$; 2100m, 2357w, 2513w, 2617 w, 2784w, 2831w, 2917sh, 2965w, 3020s cm⁻¹, ν_{CH_3} and binary bands (see refs 9 and 16). ^d SVWN5/DZVP. Infrared intensities, in km mol⁻¹, are given in parentheses, Raman intensities, in Å⁴ u⁻¹, are given in square brackets.

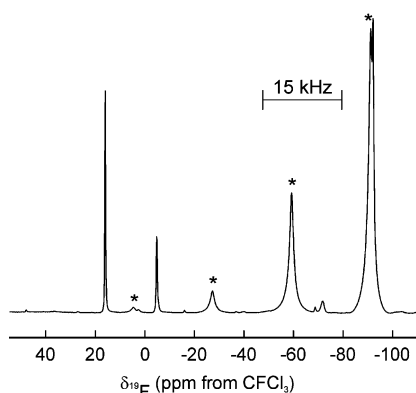


Figure 2. Solid-state ¹⁹F MAS NMR spectrum of [N(CH₃)₄]₂[IO₂F₃] containing about 75 mol% [N(CH₃)₄][F] at 15 kHz spinning rate recorded at -3 °C. Asterisks (*) denote the spinning-sideband manifold from the FEP insert material.

effect has been correlated with the decrease of the effective electronegativity on iodine.¹⁰

Solid-State NMR Spectroscopy. The insolubility of [N(CH₃)₄]₂[*cis*-IO₂F₃] precludes its solution-phase NMR spectroscopic characterization. Fluorine-19 solid-state magic-angle spinning (MAS) NMR spectra with a spinning rate of 15 kHz were recorded of a [N(CH₃)₄]₂[*cis*-IO₂F₃]-[N(CH₃)₄][F] mixture, inside a heat-sealed FEP insert. The methodology of using FEP inserts for moisture-sensitive

fluorides has previously been developed for xenon fluorides;^{17,18} the choice of FEP is based on its chemically inertness and the ease of heat-sealing FEP inserts. In addition to the FEP background signals, three resonances were observed with isotropic chemical shifts of 16.1, -4.7 ppm (approximately 2:1 ratio) and -91.9 ppm. The resonance at -91.9 ppm is attributable to [N(CH₃)₄][F]. The chemical shifts at 16.1 and -4.7 ppm can be assigned to the IF₂ and IF' groups of the IO₂F₃²⁻ anion. The shift of the more covalently bonded IF₂ moiety is close to $\delta(^{19}F)$ of [N(CH₃)₄][IO₂F₂] in CH₃CN solvent (13.7 ppm).¹⁵ A lower chemical shift of the F' is consistent with a more polar, weaker I-F' bond shifting $\delta(^{19}F)$ to the direction of F⁻ (-91.9 ppm). Proton-decoupling resulted in line widths of $\Delta\nu_{1/2} = 150$ Hz (16.1 ppm) and $\Delta\nu_{1/2} = 245$ Hz (-4.7 ppm) which did not allow for the observation of a resolved ²J(¹⁹F-¹⁹F) coupling pattern. The difference in line widths is in agreement with an unresolved doublet and triplet pattern, suggesting a maximum value of 80 Hz for the ²J(¹⁹F-¹⁹F) coupling constant. Such a value for the ²J(¹⁹F-¹⁹F) coupling constant in an iodine(V) oxide fluoride is in line with the reported coupling value for IF₅ of 85 Hz.¹⁹

The observation of relatively narrow resonances in the solid-state ¹⁹F NMR spectrum of *cis*-IO₂F₃²⁻ anion is in stark

(16) Kabisch, G. *J. Raman Spectrosc.* **1980**, *9*, 279–285.

(17) Gerken, M.; Hazendonk, P.; Nieboer, J.; Schrobilgen, G. *J. Fluorine Chem.* **2004**, *125*, 1163–1168.

(18) Gerken, M.; Hazendonk, P.; Iuga, A.; Nieboer, J.; Tramišek, M.; Goreschnik, E.; Žemva, B.; Zheng, S.; Autschbach, J. *Inorg. Chem.* **2007**, *46*, 6069–6077.

(19) (a) Bartlett, N.; Beaton, S.; Reeves, L. W.; Wells, E. J. *Can. J. Chem.* **1964**, *42*, 2531–2540. (b) Gillespie, R. J.; Quail, J. W. *Can. J. Chem.* **1964**, *42*, 2671–2673.

Table 2. Calculated Geometries of (II) and (III) Isomers of $\text{IO}_2\text{F}_3^{2-}$ and Calculated and Experimental Geometries for IO_2F_2^-

	$\text{IO}_2\text{F}_3^{2-}$ ^a		IO_2F_2^- ^b	
	isomer II	isomer III	calcd	obsd
R(I–F), pm	222.4	216.0	207.7	200.84(15)
R(I–F'), pm	206.8	228.1		
R(I–O), pm	187.8	184.3, 187.9	182.5	177.7(2), 178.0(2)
∠O–I–O, deg	97.9	100.5	109.84	106.00(12)
∠F–I–F, deg	83.9	171.9	169.26	178.39(9)

^a Calculated at the SVWN5/DZVP level of theory. ^b Data from ref 15.

contrast to the broad lines observed in the solid-state NMR spectrum of the $[\text{N}(\text{CH}_3)_4][\text{IO}_2\text{F}_2]$.²⁰ While ¹²⁷I relaxes slowly in the $[\text{N}(\text{CH}_3)_4][\text{IO}_2\text{F}_2]$ salt, fast quadrupolar relaxation is observed for the *cis*- $\text{IO}_2\text{F}_3^{2-}$ anion, resulting in self-decoupling of the ¹⁹F nucleus.

Theoretical Calculations

(a) Geometry. The geometries of the three isomers of the $\text{IO}_2\text{F}_3^{2-}$ anion were calculated using density functional theory at the SVWN5/DZVP level of theory. The C_{2v} -symmetry *trans*-isomer was found to have a single imaginary vibrational frequency, and therefore is not a local minimum. The C_s -symmetry isomers II and III were found to be local minima, with the former isomer less stable than the latter by 46 kJ/mol. The predicted gas-phase geometries of isomers II and III are summarized in Table 2, as are the calculated and experimental gas-phase geometries of the IO_2F_2^- precursor. The lower energy of isomer III is in line with larger ligand repulsion caused by the lone pair compared to that of the I–O bonds. Having one I–O bond *trans* and one *cis* to the lone pair in isomer III is favored versus both I–O bonds being *cis* to the lone pair as in isomer II. Comparison with calculated gas-phase and experimental geometry of the parent compound, IO_2F_2^- , showed that the I–F and I–O bonds elongate upon addition of F[−] to form $\text{IO}_2\text{F}_3^{2-}$, which is consistent with increased polarization of the IO and IF bonds. The I–F' bond in isomer III is weak, with a calculated bond length of 228.1 pm. The weakness of this IF' bond reflects the difficulty in forming the $\text{IO}_2\text{F}_3^{2-}$ anion and is in agreement with vibrational frequencies (see Vibrational Spectroscopy). As expected, the O–I–O and F–I–F angles in IO_2F_2^- contract upon addition of F[−]. The F–I–F angle in $\text{IO}_2\text{F}_3^{2-}$ isomer III significantly deviates from 180°.

(b) Atomic Charges. SVWN5/DZVP Löwdin atomic charges have been computed for the series IO_2F , IO_2F_2^- , $\text{IO}_2\text{F}_3^{2-}$ and are summarized in Table 3. In general, the magnitudes of the negative charges on oxygen and fluorine increase with the number of fluorine atoms *n* in $\text{IO}_2\text{F}_n^{1-n}$. This is consistent with the notion of increasing ionic character of the I–O and I–F bonds as the number of fluorine ligands *n* increases. In isomer III of *cis*- $\text{IO}_2\text{F}_3^{2-}$, the weakly bonded F' has a significantly larger negative charge (−0.66e) than the two other fluorine atoms (−0.59e), agreeing with the prediction of a rather ionic I–F' bond based on the vibrational and NMR spectroscopic data. Furthermore, in isomer III of *cis*- $\text{IO}_2\text{F}_3^{2-}$, the oxygen atom *trans* to the F'

Table 3. SVWN5/DZVP Löwdin Atomic Charges of IO_2F , IO_2F_2^- , and $\text{IO}_2\text{F}_3^{2-}$

	I	O	F
IO_2F	+1.49	−0.55	−0.39
IO_2F_2^-	+1.43	−0.69	−0.52
$\text{IO}_2\text{F}_3^{2-}$ (II)	+1.33	−0.79	−0.62 (2F), −0.51 (F')
$\text{IO}_2\text{F}_3^{2-}$ (III)	+1.41	−0.81 (O_{trans}), −0.76 (O_{cis}) ^a	−0.66 (F'), −0.59 (2F)

^a O_{trans} and O_{cis} denote the oxygen atoms *trans* and *cis* to the F' ligand, respectively.

ligand carries a larger negative charge (−0.81e) than the *cis* oxygen atoms (−0.76e), confirming the greater ionic character of the I– O_{trans} bond relative to I– O_{cis} .

(c) Vibrational Frequencies. The calculated vibrational frequencies of the two *cis*-isomers (II) and (III) of the $\text{IO}_2\text{F}_3^{2-}$ anion are listed in Table 1. The agreement between the unscaled calculated frequencies of isomer III and the experimental vibrational frequencies is reasonably good. However, the sequence of calculated $\nu_{\text{as}}(\text{IF}_2)$ and $\nu_{\text{s}}(\text{IF}_3)$ is opposite that of the experimental values. This reversed frequency sequence can be attributed to an overemphasis of I–F' involvement in $\nu_{\text{s}}(\text{IF}_3)$ stretch, which results in lowering the calculation frequency. Calculations showed that the IO stretching modes are only weakly coupled, while coupling between the IF stretching modes is more pronounced.

Conclusions

The fluoride-ion acceptor properties of IO_2F_2^- have been studied. The $[\text{N}(\text{CH}_3)_4]_2[\text{IO}_2\text{F}_3]$ salt has been prepared and characterized by solid-state ¹⁹F MAS NMR and vibrational spectroscopy in conjunction with theoretical calculations. Of the three possible isomers of the $\text{IO}_2\text{F}_3^{2-}$ anion, only the *cis*- $\text{IO}_2\text{F}_3^{2-}$ anion with a *mer*-trifluoro arrangement was observed as the exclusive product, which is a result of the repulsion caused by the lone pair. The resulting *cis*- $\text{IO}_2\text{F}_3^{2-}$ anion is presently only the second known $\text{AO}_2\text{F}_3^{n-}$ species, beside the isoelectronic XeO_2F_3^- .

Experimental Section

Materials and Apparatus. All volatile materials were handled on a Pyrex vacuum line equipped with glass/Teflon J. Young valves. Nonvolatile materials were handled in the dry nitrogen atmosphere of a dry box (Omni Lab, Vacuum Atmospheres).

Acetonitrile solvent (Baker, HPLC grade) was purified according to the standard literature method.²¹ The syntheses of $[\text{N}(\text{CH}_3)_4][\text{F}]^9$ and $[\text{N}(\text{CH}_3)_4][\text{IO}_2\text{F}_2]$ ¹⁵ have been described previously.

Preparation of $[\text{N}(\text{CH}_3)_4]_2[\text{IO}_2\text{F}_3]$. Inside a drybox, $[\text{N}(\text{CH}_3)_4][\text{IO}_2\text{F}_2]$ (0.189 mmol) and $[\text{N}(\text{CH}_3)_4][\text{F}]$ (0.754 mmol) were loaded into a 3/4 in. o.d. FEP reactor equipped with a Swagelok ORM2 stainless-steel valve and a Teflon-coated stirring bar. Approximately 4.7 mL of anhydrous CH_3CN was condensed at −196 °C onto the solid mixture and allowed to warm to −30 °C. The reaction mixture was stirred while maintained between −35 and 30 °C using an ethanol bath cooled by a Thermo NESLAB CC-100 immersion cooler for 100 h. The CH_3CN solvent was pumped off while slowly warming from −30 to 0 °C, yielding a fine, white powder consisting of $[\text{N}(\text{CH}_3)_4]_2[\text{IO}_2\text{F}_3]$ and $[\text{N}(\text{CH}_3)_4][\text{F}]$.

(20) Gerken, M.; Hazendonk, P.; Iuga, A.; Mack, J. P.; Mercier, H. P. A.; Schrobilgen, G. J. *J. Fluorine Chem.* **2006**, *127*, 1328–1338.

(21) Winfield, J. M. *J. Fluorine Chem.* **1984**, *25*, 91–98.

Vibrational Spectroscopy. The Raman spectrum of [N(CH₃)₄]₂[IO₂F₃] was recorded on a Bruker RFS 100 FT Raman spectrometer with a quartz beam splitter, a liquid-nitrogen-cooled Ge detector, and a low-temperature accessory. The backscattered (180°) radiation was sampled. The actual usable Stokes range was 50 to 3500 cm⁻¹ with a spectral resolution of 2 cm⁻¹. The 1064-nm line of an Nd:YAG laser was used for excitation of the sample. The low-temperature spectrum of [N(CH₃)₄]₂[IO₂F₃] was recorded on a powdered sample in a melting point capillary using a laser power of 200 mW. The FT-infrared spectrum of [N(CH₃)₄]₂[IO₂F₃] was recorded on a Nicolet Avatar 360 FTIR spectrometer at ambient temperature. An AgCl pellet was formed in a Wilks minipress inside the dry box by sandwiching the sample between two layers of AgCl disks. The spectra were acquired in 64 scans at a resolution of 2 cm⁻¹.

Solid-state NMR Spectroscopy. Inserts were fabricated from FEP (a copolymer of perfluorinated polypropylene and polyethylene) as previously described.¹⁷ Solid-state NMR spectra were recorded unlocked on a Varian INOVA 500 (11.744 T) spectrometer equipped with a Sun workstation. The ¹⁹F NMR spectra were obtained using a Varian 4-mm HFX MAS T3 probe tuned to 469.756 MHz. Free induction decays for the ¹⁹F spectra were accumulated with spectral width settings of 400 kHz. The number of transients accumulated for ¹⁹F spectra were 128 using pulse widths of 1 μs; relaxation delay of 2 s were applied. Proton-decoupled ¹⁹F NMR spectra were recorded using the TPPM decoupling mode. The ¹⁹F spectra were referenced to external neat CFC1₃ at room temperature.

Theoretical Calculations. Löwdin atomic charges, molecular geometries, harmonic vibrational frequencies, and infrared and

Raman vibrational intensities of the isomers of the IO₂F₃²⁻ anion were calculated using density functional theory methods. Löwdin atomic charges are obtained using a Mulliken population analysis²² based upon symmetrically orthogonalized orbitals.²³ The SVWN5 functional²⁴ (Slater exchange plus Volko-Wilk-Nusair formula 5 correlation) was used in conjunction with the double-ζ valence polarized (DZVP) basis set.²⁵ All calculations were performed using the GAMESS²⁶ quantum chemistry program.

Acknowledgment. We thank the Natural Sciences and Engineering Research Council of Canada (M.G.), the University of Lethbridge (M.G.), and the Alberta Network for Proteomics Innovation (M.G.) for support of this work. J.P.M. thanks the Natural Sciences and Engineering Research Council of Canada and the Fluorine Division of the American Chemical Society for an undergraduate research award and a Moissan fellowship, respectively. We also thank Drs. Albert Cross and Dinu Iuga for their help in the acquisition of the solid-state NMR spectra. A grant of computer time from the Department of Defense High Performance Computing Modernization Program at the Aeronautical Systems Center, Wright-Patterson Air Force Base, Ohio, is gratefully acknowledged.

IC702258X

- (22) (a) Mulliken, R. S. *J. Chem. Phys.* **1955**, *23*, 1833–1840. (b) Mulliken, R. S. *J. Chem. Phys.* **1955**, *23*, 1841–1846. (c) Mulliken, R. S. *J. Chem. Phys.* **1955**, *23*, 2338–2342. (d) Mulliken, R. S. *J. Chem. Phys.* **1955**, *23*, 2343–2346.
- (23) Löwdin, P.-O. *Adv. Chem. Phys.* **1970**, *5*, 185–199.

- (24) (a) Slater, J. C. *Phys. Rev.* **1951**, *81*, 385–390. (b) Vosko, S. H.; Wilk, L.; Nusair, M. *Can. J. Phys.* **1980**, *58*, 1200–1211.
- (25) Godbout, N.; Salahub, D. R.; Andzelm, J.; Wimmer, E. *Can. J. Chem.* **1992**, *70*, 560–571.
- (26) (a) Gordon, M. S., Schmidt M. W., as cited in Dykstra, C. E., Frenking, G. Kim, K. S. and Scuseria G. E. *Theory and Applications of Computational Chemistry: The First Forty Years*. Amsterdam: Elsevier, 2005; (b) Schmidt, M. W.; Baldridge, K. K.; Boatz, J. A.; Elbert, S. T.; Gordon, M. S.; Jensen, J. H.; Koseki, S.; Matsunaga, N.; Nguyen, K. A.; Su, S. J.; Windus, T. L.; Dupuis, M.; Montgomery, J. A. *J. Comput. Chem.* **1993**, *14*, 1347–1363.